Intramolecular Electron Transfer in Sulfite-Oxidizing Enzymes: Elucidating the Role of a Conserved Active Site Arginine[†]

Safia Emesh,[‡] Trevor D. Rapson,[§] Asha Rajapakshe,[‡] Ulrike Kappler,*[,§] Paul V. Bernhardt,[§] Gordon Tollin,*[,‡] and John H. Enemark*[,‡]

Department of Chemistry and Biochemistry, University of Arizona, Tucson, Arizona 85721, and Centre for Metals in Biology, School of Chemistry and Molecular Biosciences, The University of Queensland, Brisbane, Queensland 4072, Australia

Received August 15, 2008; Revised Manuscript Received January 14, 2009

ABSTRACT: All reported sulfite-oxidizing enzymes have a conserved arginine in their active site which hydrogen bonds to the equatorial oxygen ligand on the Mo atom. Previous studies on the pathogenic R160Q mutant of human sulfite oxidase (HSO) have shown that Mo−heme intramolecular electron transfer (IET) is dramatically slowed when positive charge is lost at this position. To improve our understanding of the function that this conserved positively charged residue plays in IET, we have studied the equivalent uncharged substitutions R55Q and R55M as well as the positively charged substitution R55K in bacterial sulfite dehydrogenase (SDH). The heme and molybdenum cofactor (Moco) subunits are tightly associated in SDH, which makes it an ideal system for improving our understanding of residue function in IET without the added complexity of the interdomain movement that occurs in HSO. Unexpectedly, the uncharged SDH variants (R55Q and R55M) exhibited increased IET rate constants relative to that of the wild type (3−4-fold) when studied by laser flash photolysis. The gain in function observed in SDH^{R55Q} and SDH^{R55M} suggests that the reduction in the level of IET seen in HSO^{R160Q} is not due to a required role of this residue in the IET pathway itself, but to the fact that it plays an important role in heme orientation during the interdomain movement necessary for IET in HSO (as seen in viscosity experiments). The pH profiles of SDH^{WT}, SDH^{R55M}, and SDH^{R55Q} show that the arginine substitution also alters the behavior of the Mo−heme IET equilibrium (K_{eq}) and rate constants (k_{et}) of both variants with respect to the SDH^{WT} enzyme. SDH^{WT} has a k_{et} that is independent of pH and a K_{eq} that increases as pH decreases; on the other hand, both SDH^{R55M} and SDH^{R55Q} have a k_{et} that increases as pH decreases, and SDH^{R55M} has a K_{eq} that is pH-independent. IET in the SDH^{R55Q} variant is inhibited by sulfate in laser flash photolysis experiments, a behavior that differs from that of SDH^{WT}, but which also occurs in HSO. IET in SDH^{R55K} is slower than in SDH^{WT}. A new analysis of the possible mechanistic pathways for sulfite-oxidizing enzymes is presented and related to available kinetic and EPR results for these enzymes.

Mo-containing metalloenzymes are found in almost all species and catalyze a diverse range of redox reactions (*1, 2*), including oxidative and reductive transformations of sulfur compounds. In vertebrate sulfur metabolism, the molybdoenzyme sulfite oxidase (SO)[1] converts toxic sulfite to sulfate in the final degradation step of the sulfur-containing amino acids cysteine and methionine (*3*). Sulfite dehydrogenase (SDH), isolated from the soil bacterium *Starkeya novella*, is a bacterial equivalent of sulfite oxidase. Unlike SO, which is necessary for detoxification of sulfite, SDH oxidizes sulfite during chemolithotrophic growth of *Starkeya novella* with thiosulfate as an energy source (*4, 5*). Despite playing different metabolic roles, both SO and SDH catalyze identical chemical reactions (eq 1) and have nearly identical active site geometries that contain several conserved residues, including C104, Y236, H57, and R55 (SDH numbering) (*6*−*8*).

$$SO_3^{2-} + H_2O + 2(\text{cyt } c)_{ox} \rightarrow SO_4^{2-} + 2(\text{cyt } c)_{red} + 2H^+ \quad \text{(i)}$$

Human SO (HSO) has been extensively studied because of its role in the genetic disease sulfite oxidase deficiency. HSO deficiency is a rare recessive metabolic neurologic disorder that presents shortly after birth (*9, 10*). The disease is characterized by seizures, dislocated ocular lenses, neuropathogenesis, and early death most likely due to a combined effect of the accumulation of toxic sulfite and glutamate, decreased sulfate concentration, and oxidative stress (*9, 11*−*14*). Point mutations in the HSO structural gene that cause the disease phenotype generally result in confor-

[†] This research was supported by NIH Grant GM-37773 (to J.H.E.). S.E. was a participant in the Undergraduate Biology Research Program, supported in part by a grant to the University of Arizona from the Howard Hughes Medical Institute (71195-5213040). T.D.R. held an Endeavor IPRS and UQ Graduate School Research Travel Grant.

* To whom correspondence should be addressed. J.H.E.: e-mail, jenemark@u.arizona.edu; phone, (520) 621-2245; fax, (520) 626-8065. U.K.: e-mail, u.kappler@uq.edu.au; phone, (07) 3365 2978; fax, (07) 3365 4620. G.T.: e-mail, gtollin@u.arizona.edu; phone, (520) 621-3447; fax, (520) 621-9288.

[‡] University of Arizona.

[§] The University of Queensland.

[1] Abbreviations: CSO, chicken sulfite oxidase; dRF, 5-deazariboflavin; HSO, human sulfite oxidase; IET, intramolecular electron transfer; k_{et}, electron transfer rate constant; K_{eq}, equilibrium constant for intramolecular electron transfer; Moco, molybdenum cofactor; SDH, sulfite dehydrogenase; SO, sulfite oxidase.

10.1021/bi801553q CCC: $40.75
Published on Web 02/18/2009

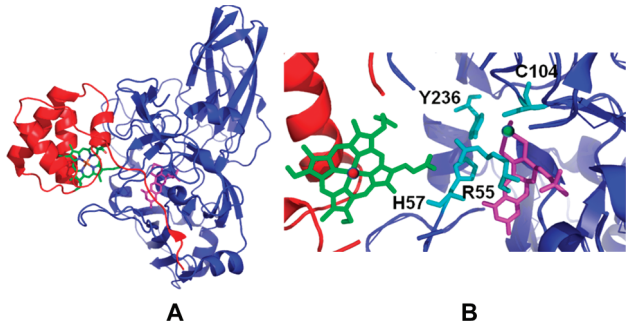

FIGURE 1: (a) Crystal structure of SDH showing that the SorB subunit (red) and the SorA subunit (blue) are tightly bound. The distance between the heme iron atom (green) located in the SorB subunit and the Moco molybdenum atom (purple) in the SorA subunit is ~16.6 Å. (b) Active site of SDH^{WT} showing the Moco (Mo colored green) and heme (Fe colored red) cofactors and conserved residues H57, R55, C104, and Y236 (Protein Data Bank entry 2bpb).

mational changes in and around the active site or the disruption of the dimeric structure of HSO to give inactive monomeric subunits. Active site mutations can affect the coordination of the molybdenum cofactor (Moco), the active site geometry, and enzyme turnover rates and cause decreased intramolecular electron transfer (IET) rates (*15, 16*).

Although SO and SDH catalyze the same reaction, there are several key differences between them which make the latter an important enzyme for studying IET. The crystal structure of SDH (Figure 1A) shows that, unlike chicken SO (CSO), the heme and Mo cofactors are located on separate subunits that are "locked" by a high-affinity interaction between the subunits (*7*). In SO, the heme and Mo domains are linked by a flexible loop with no secondary structure, and catalysis requires a conformational change to position the heme and Mo domains sufficiently close to one another. This interdomain movement is a necessary step for IET as observed by Feng et al. (*17*), who showed that the rate constant of IET decreased linearly by the negative 0.7th power of viscosity. In identical experiments with SDH (*18*), increased viscosity did not affect either the equilibrium constant or the rate constant of IET. This suggests that there is no significant subunit movement or a subunit "docking" step in SDH that could be retarded by a viscogen (*18, 19*), and that IET occurs through the protein and/or solvent interface between the two locked subunits which have a Mo···Fe distance of ~16 Å (*7*). The closest approach of the two cofactors (8.5 Å) occurs between the molybdenum atom and propionate 6 of the heme and is well within typical distances for rapid electron tunneling in proteins (*20*). Others have emphasized that optimum electronic coupling pathways between the redox sites can often be identified within the protein structure (*21*). For SDH, two IET pathways have been proposed (*7*). One pathway involves Arg55 and the hydrogen bonding network to the heme propionate groups, which are located directly between the two redox centers. The second pathway involves a series of aromatic residues that span the space between the two redox centers. The crystal structure of SDH shows that F168 of the molybdenum-containing subunit stacks against the aromatic pterin cofactor and Y61 of the heme subunit stacks against the pyrrole D-ring. The intervening space is occupied by Y236, W231, and F230 of the molybdenum-containing subunit; all aromatic residues in the proposed pathway have edge-to-edge distances of ~4 Å (*7*).

Making amino acid substitutions along each proposed pathway should provide insight about the IET process in SDH and, by implication, in the hypothesized "docked" form of HSO. Another advantage of SDH is that unlike HSO, intact SDH can be crystallized so that the effects of amino acid substitutions on the active site environment can also be studied by X-ray diffraction.

This study is the first to compare an HSO variant known to cause SO deficiency (R160Q) to an equivalent substitution in SDH (R55Q and R55M). From the human R160Q studies, it was found that at pH 6.0 the IET rate constant decreased from 411 s^{-1} in HSO^{WT} to 0.64 s^{-1} in HSO^{R160Q} and that a partial restoration of the rate constant (to 96 s^{-1}) could be obtained with an R160K substitution (*22*). Thus, the positive charge at this location in the HSO active site is important for facilitating IET (*15, 22*). Mechanistically, the R160 residue could be involved in the pathway of IET or could be a necessary residue to aid in heme reorientation during interdomain movement. The equivalent R55K substitution in SDH further explores the importance of the positive charge at this position in IET.

This investigation of the laser flash photolysis kinetic profile of SDH^{WT} and the IET rate constants of SDH^{R55M}, SDH^{R55Q}, and SDH^{R55K} provides essential benchmark data for evaluating the role of R55 in the pathway for IET in SDH. By implication, these results for SDH which has a locked interaction between the Mo and heme domains should also enable the mechanistic role of R160 in HSO and inherited SO deficiency to be addressed. In addition, we provide laser flash photolysis kinetic data on the effects of anion inhibition on SDH^{R55Q}. Anions are known to effectively inhibit IET in SO (*23*−*25*).

MATERIALS AND METHODS

Molecular Biology. The generation of SDH^{R55M} has been reported previously (*26*). SDH^{R55Q} and SDH^{R55K} were generated by using primer pairs R55Q_fwd (GAC GCC TTC TTC GTG *CAG* TAC CAT CTC GCC GGT) and R55Q_rev (ACC GGC GAG ATG GTA *CTG* CAC GAA GAA GGC GTC), and R55K_fwd (GAC GCC TTC TTC GTG *AAG* TAC CAT CTC GCC GGT) and R55K_rev (ACC GGC GAG ATG GTA *CTT* CAC GAA GAA GGC GTC) essentially as described in ref *27*. The presence of the mutations was verified by DNA sequencing at all stages of cloning.

Protein Purification. SDH^{R55M}, SDH^{R55Q}, and SDH^{R55K} were expressed in *Rhodobacter capsulatus* and purified using previously developed procedures for SDH proteins (*28*).

Steady State Assays. Extensive studies with SDH^{WT} and SDH^{R55M} have been published (*26*). Steady state data for SDH^{R55Q} and SDH^{R55K} were obtained using the same protocols.

Laser Flash Photolysis. The pH profile laser flash photolysis studies with SDH^{WT}, SDH^{R55M}, SDH^{R55Q}, and SDH^{R55K} were carried out at pH 6.0, 5.5, and 5.1 in 20 mM Bis-Tris acetate buffer; 300 μL of buffer containing an ~90 μM freshly prepared 5-deazariboflavin (dRF) solution was made anaerobic by bubbling with argon gas for ~2 h. A concentrated drop of protein was deaerated by blowing argon

gas across its surface and was then mixed into the dRF buffer. Data were collected at room temperature for protein concentrations of 10, 15, and 20 μM to ensure that the rate constant was independent of protein concentration, as expected for an intramolecular reaction.

The sulfate inhibition experiments were performed using the same buffers mentioned above with a SDH^{R55Q} protein concentration of 10 μM. Data were collected at sulfate concentrations of 0, 25, 50, and 100 mM. In these experiments, a concentrated drop of sulfate solution was deaerated and then mixed into the dRF solution. The data were collected at room temperature, and the addition of sulfate did not change the pH of the buffer.

The effect of 0, 12.5, 25, 50, and 100 mM acetate [added from a 1.6 M stock solution of sodium acetate buffer (pH 5)] on IET was tested at pH 5 in 20 mM Bis-Tris acetate buffer that contained 10 μM SDH^{R55Q} as described above.

The intramolecular electron transfer rates were determined by laser flash photolysis, using a previously described procedure (*17*−*19*). A nitrogen-pumped dye laser (7 mJ, 10 ns/pulse, $\lambda = 398$ nm) excited 5-deazariboflavin (dRF) to the triplet state (eq 1). The ^{3}dRF was then reduced to the semiquinone radical (dRFH$^\bullet$) by semicarbazide (AH_2 in eq 2). The radical reduced the heme from Fe(III) to Fe(II), as seen by an increased absorbance at 553 nm (eq 3). A decrease in absorbance followed as Fe(II) transferred an electron via IET to Mo(VI), and an equilibrium was reached between the Mo(VI)Fe(II) and Mo(V)Fe(III) forms of the enzyme (eq 4).

$$\mathrm{dRF} \xrightarrow{h\nu} {}^3\mathrm{dRF} \tag{1}$$

$$^3\mathrm{dRF} + \mathrm{AH_2} \rightarrow \mathrm{dRFH^\bullet} + \mathrm{AH^\bullet} \tag{2}$$

$$\mathrm{dRF^\bullet} + \mathrm{Mo^{VI}Fe^{III}} \rightarrow \mathrm{dRF} + \mathrm{Mo^{VI}Fe^{II}} \tag{3}$$

$$\mathrm{Mo^{VI}Fe^{II}} \underset{k_r}{\overset{k_f}{\rightleftharpoons}} \mathrm{Mo^{V}Fe^{III}} \tag{4}$$

The IET rate constant can be calculated by fitting the heme reoxidation curve with an exponential function (eq 5) where the IET rate constant is the sum of the forward and reverse electron transfer rate constants (k_f and k_r, respectively, in eq 6).

$$\frac{dA_{553}}{dt} = a + b^{\exp(-k_{et}t)} \tag{5}$$

$$k_{et} = k_f + k_r \tag{6}$$

The equilibrium constant can then be calculated using the parameters a and b, which are determined from the kinetic traces.

$$a = A_o\frac{k_r}{k_{et}} = A_o\frac{k_r}{k_f + k_r} \tag{7}$$

$$b = A_o\frac{k_f}{k_{et}} = A_o\frac{k_f}{k_f + k_r} \tag{8}$$

$$K_{eq} = \frac{k_f}{k_r} = \frac{b}{a} \tag{9}$$

The forward and reverse rate constants (k_f and k_r, respectively) of IET can then be calculated from the equilibrium constant (eq 9), thereby providing quantitative information about both the forward and reverse rates of electron transfer in the enzyme. Note that k_f in these flash photolysis experiments is actually the reverse of the physiological IET direction.

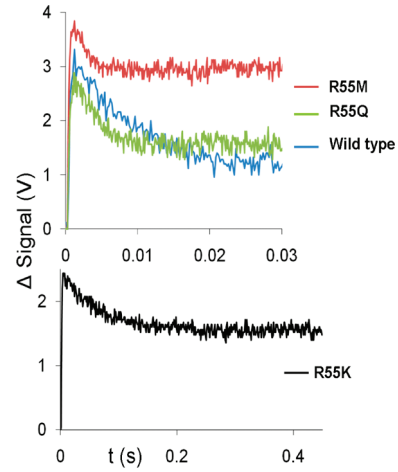

FIGURE 2: (Top) Laser flash photolysis kinetic traces of SDH^{WT}, SDH^{R55Q}, and SDH^{R55M} showing that SDH^{R55M} (red trace) has the fastest IET kinetics (largest k_{et}) but the smallest K_{eq}. (Bottom) Laser flash photolysis trace for SDH^{R55K}; note the longer time scale. All experiments were performed with 20 μM protein in a buffer containing 20 mM Bis-Tris acetate, 0.5 mM semicarbazide, and ~90 μM dRF at pH 5.1.

Table 1: Laser Flash Photolysis Kinetic and Equilibrium Data from pH Profiles

		pH 5.1	pH 5.5	pH 6.0
SDH^{WT}	k_{et} (s^{-1})	123 ± 5	124 ± 3	122 ± 5
	k_f (s^{-1})	75 ± 3	61 ± 1	56 ± 2
	k_r (s^{-1})	48 ± 2	63 ± 1	66 ± 3
	K_{eq}	1.57 ± 0.05	0.98 ± 0.02	0.85 ± 0.04
SDH^{R55Q}	k_{et} (s^{-1})	377 ± 22	371 ± 20	293 ± 20
	k_f (s^{-1})	165 ± 10	150 ± 8	87 ± 6
	k_r (s^{-1})	212 ± 12	221 ± 12	206 ± 14
	K_{eq}	0.78 ± 0.01	0.68 ± 0.02	0.42 ± 0.02
SDH^{R55M}	k_{et} (s^{-1})	535 ± 44	460 ± 51	217 ± 25
	k_f (s^{-1})	100 ± 8	95 ± 10	33 ± 4
	k_r (s^{-1})	435 ± 35	365 ± 40	184 ± 20
	K_{eq}	0.23 ± 0.03	0.26 ± 0.03	0.18 ± 0.01
SDH^{R55K}	k_{et} (s^{-1})	15 ± 0.7	16 ± 1.7	–
	k_f (s^{-1})	5.6 ± 0.3	4 ± 0.4	–
	k_r (s^{-1})	9.4 ± 0.4	12 ± 1	–
	K_{eq}	0.59 ± 0.02	0.34 ± 0.03	–

RESULTS AND DISCUSSION

Kinetics of IET. Initial laser flash photolysis experiments with SDH^{WT} performed previously by Feng et al. (*18*) found that IET could not be observed at pH 7.4, the pH at which IET for HSO is generally studied. In SDH^{WT}, IET was observed only when the pH was lowered to 6 (*18*) where the redox potential of Mo(VI) becomes more positive than that of the heme, allowing electron transfer from Fe(II) to Mo(VI) (*29*). In the study presented here, we have extended this work to the SDH arginine 55 variants that are related to the HSO^{R160Q} mutation. Typical kinetic traces for SDH^{WT} and the R55 SDH variants are shown in Figure 2. The overall rate of IET for SDH^{WT} was found to be unaffected by pH (Table 1), unlike the equilibrium constant which nearly doubled as the pH was decreased from pH 6 to 5.1, which means that the forward rate constant (k_f) increased according

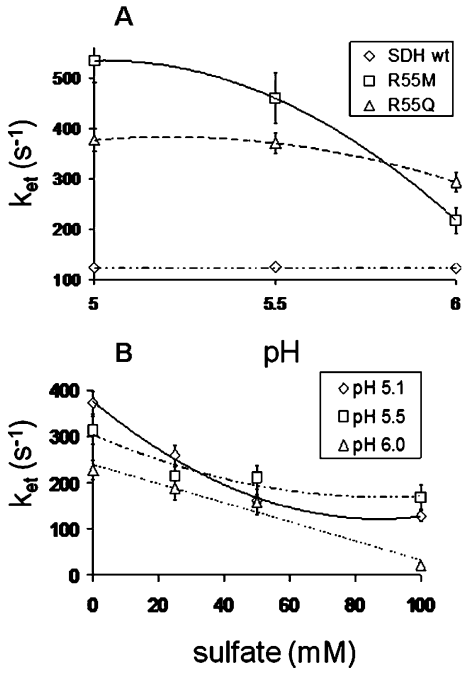

FIGURE 3: (A) pH profiles of SDH^{WT}, SDH^{R55Q}, and SDH^{R55M}. SDH^{WT} shows no pH dependence and a rate constant of ~120 s^{-1}. Both SDH^{R55Q} and SDH^{R55M} show pH dependence and rate constants much higher than that of SDH^{WT} across the pH range. (B) Sulfate inhibition experiment with SDH^{R55Q} showing that the IET rate constant decreases with an increase in sulfate concentration at several pH values, a trend not observed in SDH^{WT}.

to eq 7. It is important to note that the forward reaction in laser flash experiments is in the opposite direction of enzyme turnover. The overall IET rate constant, however, remained unaffected by pH due to a corresponding decrease in the reverse rate constant (see also Figure 3A). The value of k_{et} at pH 6 was about twice as large as k_{cat} under these conditions (*26*), confirming that IET is not the rate-limiting step for SDH^{WT} (*18*).

The SDH^{R55Q} variant has the same Arg to Gln substitution that is observed in the fatal disease sulfite oxidase deficiency (R160Q) in humans. HSO^{R160Q} shows a markedly decreased IET rate constant compared to that of HSO^{WT} (by a factor of almost 400-fold), suggesting that the electrostatic effects of this residue are important for IET to occur in HSO (*22*). However, for SDH^{R55Q}, Table 1 shows that k_{et} is ~3 times *larger* than that for SDH^{WT}. Both K_{eq} and k_{et} were mildly pH dependent. The forward IET rate constant increased with a decrease in pH, but the reverse rate constant was unchanged across the pH range. K_{eq} increased with a decrease in pH, with a 2-fold increase in K_{eq} at pH 5.1 compared to that observed at pH 6. Note that the K_{eq} trend obtained in SDH^{R55Q} is the same trend observed in SDH^{WT}. The SDH^{R55Q} variant has lost a positive charge at the active site, but the oxygen atom of the Gln residue can hydrogen bond to nearby proton donors and water molecules at the active site.

The replacement of Arg55 with Met, which cannot have hydrogen bonding interactions, had an interesting and unexpected effect on the IET rate (Table 1). For SDH^{R55M}, the IET rate constant was 2-fold larger than in SDH^{WT} at pH 6. Furthermore, the rate became pH-dependent and increased as the pH was lowered. At pH 5.1, the IET in SDH^{R55M} was found to be 4-fold faster than in SDH^{WT}. Additionally, for SDH^{R55M}, the IET rate constant became pH-dependent but K_{eq} became approximately pH independent, the opposite of what was observed in SDH^{WT}. Therefore, for SDH^{R55M}, both the forward and reverse IET rate constants increased with a decrease in pH. This raises the possibility that SDH^{R55M} has a more efficient tunneling pathway for IET (*21*).

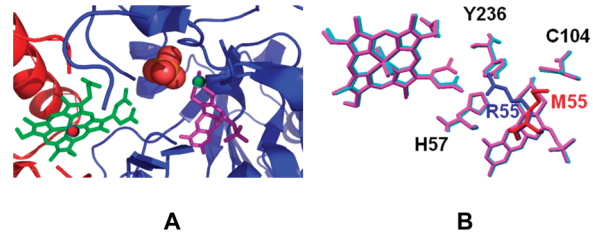

FIGURE 4: (A) SDH^{R55M} with sulfate bound in the active site. (B) Overlay of the active sites of SDH^{WT} (cyan) and SDH^{R55M} (purple). For SDH^{WT}, the R55 residue (blue) has its side chain extending into the active site. In SDH^{R55M}, the M55 residue (red) is bent away from the active site, leaving the position occupied by R55 empty (Protein Data Bank entry 2ca3).

The recently published crystal structure of SDH^{R55M} shows a dramatic change in the active site compared to SDH^{WT}. The M55 residue is bent away from the active site, and the position previously occupied by R55 in SDH^{WT} is empty (Figure 4B) (*26*). This structural result and the IET experiments suggest that the positive charge of the R55 side chain actually decreases the IET rate by its location in the region between the heme and the molybdenum and also modifies the K_{eq}. We have previously pointed out that an altered proton environment about the molybdenum center may affect the electronic coupling between the Mo(VI/V) and Fe(III/II) centers and thereby change the kinetics of IET (*27*). A theoretical analysis of aqueous tunneling pathways for electron transfer between redox cofactors in two separate protein domains showed that the rates of electron transfer are highly dependent on the structure of the intervening water molecules at their interface (*30*). A change in the structure of the water molecules between the Mo and heme cofactors could be a factor in the higher IET rate for SDH^{R55M} compared to that of SDH^{WT}.

Another feature of the SDH^{R55M} structure that differs from SDH^{WT} [and from both SDH^{Y236F} (*27*) and SDH^{H57A} (*26*)] is the association of a sulfate anion with the active site (Figure 4A). When crystallized in the presence of sulfate, the structures of CSO^{WT} and the Mo domain of CSO^{R138Q} also show sulfate associated with the active site (*15, 16*). There is no crystal structure available for SDH^{R55Q}, but pulsed EPR studies following reduction with ^{33}S-labeled sulfite show that this variant has sulfate coordinated to the Mo atom (A. V. Astashkin, T. D. Rapson, U. Kappler, and J. H. Enemark, unpublished experiments). The presence of sulfate either loosely associated with the active site (SDH^{R55M}) or directly coordinated to the Mo (SDH^{R55Q}) may have implications for the IET behavior of these variants. This was tested in the experiments described below.

A laser flash photolysis sulfate inhibition experiment was performed to test if the active site of SDH^{R55Q} was altered substantially enough so that the enzyme had increased sensitivity to small anions in solution. SDH^{WT} does not show any inhibition of IET at sulfate concentrations as high as 55 mM (*18*). When this same experiment was performed on SDH^{R55Q}, there was a distinct decrease in the IET rate

Table 2: Laser Flash Photolysis Kinetic and Equilibrium Data Obtained from Sulfate Inhibition Experiments on SDH^{R55Q}

		0 mM sulfate	25 mM sulfate	50 mM sulfate	100 mM sulfate
pH 5.1	k_{et} (s^{-1})	372 ± 24	260 ± 21	161 ± 12	128 ± 12
	k_f (s^{-1})	154 ± 10	100 ± 8	49 ± 4	42 ± 4
	k_r (s^{-1})	218 ± 14	160 ± 13	112 ± 8	86 ± 8
	K_{eq}	0.71 ± 0.01	0.62 ± 0.06	0.44 ± 0.03	0.48 ± 0.03
pH 5.5	k_{et} (s^{-1})	313 ± 30	225 ± 20	212 ± 26	168 ± 26
	k_f (s^{-1})	91 ± 9	56 ± 5	35 ± 4	24 ± 4
	k_r (s^{-1})	222 ± 21	159 ± 15	177 ± 22	144 ± 22
	K_{eq}	0.41 ± 0.03	0.35 ± 0.06	0.2 ± 0.04	0.17 ± 0.02
pH 6.0	k_{et} (s^{-1})	228 ± 21	188 ± 25	158 ± 28	21 ± 6
	k_f (s^{-1})	58 ± 5	35 ± 5	22 ± 4	2 ± 0.6
	k_r (s^{-1})	170 ± 16	153 ± 20	136 ± 24	19 ± 5
	K_{eq}	0.34 ± 0.03	0.23 ± 0.004	0.16 ± 0.01	0.13 ± 0.03

constant at pH 5.1, 5.5, and 6.0 in the presence of sulfate (Table 2 and Figure 3B). The sulfate inhibition effects are similar to what was observed with chicken SO (*24*); i.e., at high concentrations of sulfate (10000-fold excess of sulfate over enzyme concentration), the rate constants decreased appreciably. This shows that although the sulfate bound in the active site does not completely inhibit the enzyme, when sulfate is bound the enzyme is in a less active state. Presumably, when the sulfate dissociates, activity is restored.

To test if the IET sulfate inhibition was the result of nonspecific electrostatic interactions that result from a high ionic strength, a laser flash photolysis inhibition study was performed using acetate as the anion. There was no change in the IET rate constant with an increase in acetate concentration until the acetate concentration reached 100 mM, a 10000-fold excess of acetate over enzyme, at which concentration an approximately 20% decrease was observed. This shows that like HSO and CSO, the sulfate anion inhibition in SDH^{R55Q} is a specific interaction in the active site, whereas larger anions such as acetate have no effect on IET except at very high concentrations where nonspecific ionic strength effects may occur (*23*).

In view of the enhanced IET rates for SDH^{R55M} and SDH^{R55Q}, the SDH^{R55K} variant was prepared to further explore the effect of the positive charge of R55 on both IET rates and steady state kinetics. Table 1 and Figure 2 show that the SDH^{R55K} variant has IET rates which are much slower than those of SDH^{R55M} and SDH^{R55Q}. This behavior of SDH^{R55K} contrasts with that of the analogous R160K variant in HSO, which exhibits much faster IET rates than HSO^{R160Q}. The overall rate of IET for SDH^{R55K} was unchanged as the pH was varied from 5.1 to 5.5, similar to the trend observed for SDH^{WT}. The IET rate constant for the SDH^{R55K} variant at pH 6.0 could not be determined reliably. The forward IET rate constant decreased with an increase in pH, whereas the reverse IET rate constant increased, thereby resulting in an approximately 2-fold increase in K_{eq} with a decrease in pH. The IET data for SDH^{R55K} further support the hypothesis that a primary role of the positive charge of R160 in HSO is to aid in docking the negatively charged propionate groups of the heme domain. The steady state kinetics of SDH^{R55K} (Table 3) show smaller values of $k_{cat,app}$ and larger values of $K_{Msulfite,app}$ compared to those of SDH^{WT}. The catalytic efficiency ($k_{cat}/K_{Msulfite}$) of SDH^{R55K} is ~2 orders of magnitude smaller than that of SDH^{WT} but 2 orders of magnitude larger than that of the SDH^{R55M} or SDH^{R55Q} variant, each of which lacks a positive charge at the active site. SDH^{R55M} and SDH^{R55Q} also have much larger values of $K_{Msulfite,app}$ than SDH^{R55K}, consistent with the proposal that the positively charged R55 plays an important role in substrate binding and product release (*26*). No crystal structure of SDH^{R55K} is yet available to evaluate the hydrogen bonding interactions of 55K within the active site.

Table 3: Steady State Assays

	pH	$K_{Msulfite}$ (μM)	k_{cat} (s^{-1})	$k_{cat}/K_{Msulfite}$ (M^{-1} s^{-1})	ref
SDH^{WT}	6.0	0.6 ± 0.01	63.5 ± 2.2	1.1×10^8	*26*
	8.0	22 ± 0.3	345 ± 11	1.6×10^7	
SDH^{R55Q}	6.0	2250 ± 247	41 ± 1.5	1.8×10^4	this work
	8.0	39200 ± 17800	108 ± 35	2.8×10^3	
SDH^{R55M}	6.2	1087 ± 260	64 ± 3.9	5.9×10^4	*26*
	7.9	8170 ± 1370	73.4 ± 4.8	3.3×10^3	
SDH^{R55K}	6.0	8.9 ± 1.4	17 ± 0.61	1.9×10^6	this work
	8.0	230 ± 22	160 ± 7	7.0×10^5	

All three SDH variants exhibit values of K_{eq} smaller than that of SDH^{WT} (Table 1) at all pH values. These data indicate that for these variants eq 4 is shifted to the left relative to SDH^{WT}, which implies changes in the reduction potentials of the components. The shift in equilibrium could result from the Mo(VI/V) couple becoming less positive, from the Fe(III/II) couple becoming more positive, or from complicated changes involving both metal centers. Unlike the situation for SDH^{WT} (*31*), repeated attempts to directly measure the reduction potentials of the metal centers of the SDH R55 variants by protein film voltammetry (PFV) (*32*) were unsuccessful, thereby preventing a direct electrochemical analysis of the changes in the molybdenum and heme potentials. Measurement of the Mo(VI/V) potentials by EPR titrations (*27*) was also not feasible because of the large amount of protein required. An additional complication of EPR titrations is that freezing the solutions can change the pH and thereby change the potential (Table 1). However, the values of K_{eq} in Table 1 enable the potential difference between Fe(III/II) and Mo(VI/V) ($\Delta\varepsilon^0$) to be determined for the overall reaction of eq 4 for each variant at each pH. Additionally, UV−vis titration experiments show that the heme Fe(III/II) potential is little affected by the R55 substitutions (T. D. Rapson, U. Kappler, and P. Bernhardt, unpublished data). Thus, combining $\Delta\varepsilon^0$ for the overall reaction with the known value of the heme reduction potential (~200 mV) enables the potential of the Mo(VI/V) couple to be calculated for each set of conditions in Table 1. The largest value of K_{eq} is 1.57 for SDH^{WT} at pH 5.2. This gives a $\Delta\varepsilon^0_{reaction}$ of 12 mV and a Mo(VI/V) potential of 196 mV. It must be pointed out that the Mo(VI/V) potential determined for SDH^{WT} at pH 5.2 by direct voltammetry (381 mV) (*31*)

is much larger than that calculated here. Although the reason for the large difference between the Mo(VI/V) potentials determined through PFV and potentiomery is not known at present, it should be remembered that the two techniques are fundamentally different. A PFV measurement requires adsorption of the protein on an electrode surface and, in the case of SDH^{WT}, immobilized within a surfactant film. Due to differences in solvation of the redox cofactors and perhaps protein conformational changes caused by adsorption in a PFV experiment, the apparent redox potentials do not necessarily mirror those determined in solution using redox potentiometry. Further intrinsic difficulties in PFV potential measurements include the reproducibility of the graphite electrode surface and the low signal-to-noise ratio. Nonetheless, PFV studies of SDH show electrocatalytic oxidation of sulfite (*31*). This result indicates that both metal cofactors of SDH remain associated with the protein within the surfactant film. For chicken SO, the potential of the heme center was successfully determined by PFV, and the electrocatalytic oxidation of sulfite was studied even though the molybdenum potential could not be observed (*33*). Redox potentiometry is a less invasive, solution-based measurement in which spectral changes accompanying reduction and oxidation support the assignment of each oxidation state, highlighting an inherent and unavoidable drawback of PFV. However, the nearly equipotential Mo(VI/V) and Fe(III/II) couples found here are consistent with facile IET as well as transfer to cytochrome *c*. The smallest value of K_{eq} is 0.18 for SDH^{R55M} at pH 6.0, which gives a $\Delta\varepsilon^0_{reaction}$ of −44 mV and a Mo(VI/V) potential of 156 mV.

Mechanistic Considerations. The oxidation of sulfite by SDH is a two-electron process. The catalytic cycle proposed for SDH (*26*) is analogous to that originally suggested for SO (*3, 34*). Oxidized SDH [Mo(VI)] reacts with sulfite to form reduced SDH [Mo(IV)] and the product (sulfate). Two subsequent sequential one-electron oxidations then return the Mo center to the Mo(VI) form. These one-electron oxidation steps involve IET to the heme domain of the enzyme which in turn is oxidized by exogenous cytochrome *c*. However, these studies of the R55 variants of SDH suggest that other catalytic pathways also need to be considered for SDH and other sulfite-oxidizing enzymes.

Scheme 1 presents a more general view of sulfite oxidation catalyzed by SDH and the possible pathways available for the enzyme−substrate complex to ultimately form product (sulfate) and the reoxidized Mo(VI) state of the enzyme. The prevailing view (*3, 19, 34*) has been that the reaction proceeds by release of sulfate from the enzyme−substrate complex (k_2) followed by two sequential one-electron oxidations of the Mo center (k_4 and k_7). This entire sequence is colored red in Scheme 1.

A second possibility would be for the enzyme−substrate complex to be oxidized by one electron (k_3 in Scheme 1) followed by product dissociation (k_5) and then oxidation by one electron (k_7). This sequence is colored blue. For SDH^{WT} and the R55 variants, IET rates are significantly faster than catalytic turnover which strongly supports the second pathway colored blue as the dominant one for SDH. Direct evidence for a one-electron oxidized enzyme−substrate complex, i.e., the $Mo^V(OSO_3^{2-})$ species of Scheme 1, has been obtained from pulsed EPR studies of HSO^{R160Q} that has been reduced by sulfite labeled with ^{33}S ($I = {}^3/_2$) (*35*).

Scheme 1: Possible Reaction Pathways for the Catalytic Oxidation of Sulfite by SDH or SO[a]

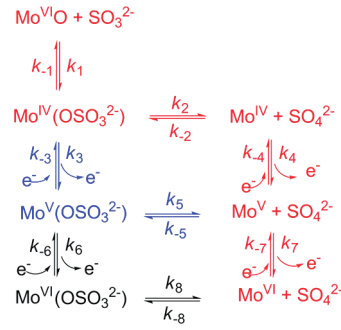

[a] For the sake of simplicity, the enzyme and substrate are depicted as $Mo^{VI}O$ and SO_3^{2-}, respectively. The pathways differ in the sequence of steps which transform the enzyme−substrate complex, $Mo^{IV}(OSO_3^{2-})$, into product (sulfate) and the reoxidized Mo(VI) state of the enzyme. The pathway colored red is the one commonly proposed, in which product release precedes reoxidation of the enzyme. For the pathway colored blue, the enzyme−substrate complex is oxidized by one electron prior to product release. For the pathway colored black, the enzyme−substrate complex is oxidized by two electrons prior to product release. See the text for additional discussion.

A third possibility of Scheme 1 is for the enzyme−substrate complex to be oxidized by two electrons to Mo(VI) (k_3 and k_6) before release of sulfate (k_8), as shown in the pathway colored black. The kinetics of the SDH^{Y236F} variant are consistent with this pathway. This variant is catalytically competent even though it does not exhibit IET by flash photolysis (steps k_7 and k_{-7}) (*27*).

Scheme 1 was developed from considering kinetic data for several SDH variants. However, since Scheme 1 focuses solely on the Mo atom oxidation state and the release of sulfate from the enzyme−substrate complex, it should also be applicable to SO from animal and plant sources. During catalytic turnover, more than one of the pathways of Scheme 1 may be operative, which would complicate interpretation of kinetic results. Changing the pH or ionic strength and mutating residues around the active site could alter which pathway is more favorable. It was previously suggested that the two conformations of the heme propionate groups in the crystal structure of SDH^{R55M} might result in more than one catalytic pathway (*26*). Scheme 1 enables such a proposal to be rationalized.

For SDH and vertebrate SO, the IET step that has been studied by flash photolysis relates the Mo(VI) and Mo(V) forms of the enzyme in the absence of substrate (or product). Thus, k_7 and k_{-7} of Scheme 1 correspond to k_r and k_f of eq 6, respectively. As noted earlier, IET is usually much faster than turnover and not the rate-determining step. However, SDH provides a naturally occurring protein system with a fixed arrangement of donor and acceptor in which the intervening medium of amino acid residues and hydrogen bonds can be systematically varied by site-directed mutagenesis to provide important insights concerning IET.

CONCLUSION

SDH^{R55M} and SDH^{R55Q} are the first active site variants of any sulfite-oxidizing enzyme to exhibit an increased IET rate constant. This is especially surprising because the equivalent HSO^{R160Q} variant shows a dramatic decrease in the IET rate

constant. These results indicate that the conserved active site arginine residue found in SDH and SO is not a required part of the electron transfer pathway between the heme and Moco, while being consistent with the positive charge influencing the docking between the heme and molybdenum domains in SO (*22*). However, the IET kinetics presented here for SDH^{WT} and the R55 variants do not distinguish between the two previously proposed IET pathways: (1) a hydrogen bonding network involving R55 and the heme propionate groups and (2) a series of aromatic residues between the redox centers (*7*). Clearly, the results for R55 and K55 show that the presence of a positive charge at this position influences IET in SDH in a negative way, and this may be important in regulating electron transfer. For example, a positively charged residue at position 55 near the active site could affect IET by controlling the Mo(VI/V) potential. Another possibility is that the positive charge affects the local water structure and hence the aqueous electron tunneling pathways between the two redox centers (*30*). Previous kinetic studies of SDH catalysis have shown that the R55 residue is important for effective substrate binding, and the $K_{Msulfite,app}$ for SDH^{R55M} is 2−3 orders of magnitude larger than that for SDH^{WT}. Consistent with these earlier studies, $K_{Msulfite,app}$ for SDH^{R55K} is only a factor of ∼10 larger than that for SDH^{WT} (Table 3).

SDH variants with substitutions of aromatic amino acids along the second proposed pathway for IET (*7*) have not been systematically investigated. However, the SDH^{Y236F} variant exhibited reduced turnover rates and substrate affinity, and no quantifiable IET was seen in laser flash photolysis experiments (*27*). Substitution of the active site tryptophan that is conserved in sulfite-oxidizing enzymes (W231 in SDH) could have interesting IET consequences because very recent studies show that tryptophan residues can play a key role in hopping mechanisms of IET (*36*).

Biological electron transfer remains an area of intense experimental and theoretical interest. Recent theoretical studies have emphasized that constructive and destructive interference among multiple pathways can play a major role in the overall rate of electron transfer in proteins. In one such study, it was found that methionine provides an efficient pathway for electron transfer (*37*−*39*), a result that is reminiscent of what we observed in this work for SDH^{R55M}. The importance of protein dynamics in electron transfer rates is also receiving an increased level of attention. A very recent theoretical paper indicated that fluctuation contributions dominate the tunneling mechanism in proteins at distances beyond 6−7 Å. Nonetheless, the protein fold is "remembered" by the electronic coupling, and structure remains a key determinant of electron transfer kinetics (*40*). We reiterate that SDH is a naturally occurring protein system with a fixed arrangement of donor and acceptor in which the intervening medium of amino acid residues and hydrogen bonds can be systematically varied by site-directed mutagenesis to provide important insights concerning IET. Finally, SDH provides a model for the proposed docking of the molybdenum and heme domains of human SO during catalysis. Thus, studies of SDH may also provide insight concerning mutations of human SO that lead to fatal sulfite oxidase deficiency.

ACKNOWLEDGMENT

We thank Drs. Kayunta Johnson-Winters and Robert Berry for helpful discussions.

REFERENCES

1. Schwarz, G., and Mendel, R. R. (2006) Molybdenum Cofactor Biosynthesis and Molybdenum Enzymes. *Annu. Rev. Plant Biol. 57*, 623–647.
2. Hille, R. (2002) Molybdenum and Tungsten in Biology. *Trends Biochem. Sci. 27*, 360–367.
3. Rajagopalan, K. V. (1980) Sulfite Oxidase (Sulfite: Ferricytochrome *c* Oxidoreductase). in *Molybdenum and Molybdenum-Containing Enzymes* (Coughlan, M. P., Ed.) Pergamon Press, Oxford, U.K.
4. Kappler, U., Friedrich, C. G., Truper, H. G., and Dahl, C. (2001) Evidence for Two Pathways of Thiosulfate Oxidation in *Starkeya Novella* (Formerly *Thiobacillus Novellus*). *Arch. Microbiol. 175*, 102–111.
5. Kelly, D. P., McDonald, I. R., and Wood, A. P. (2000) Proposal for the Reclassification of *Thiobacillus Novellus* as *Starkeya Novella* gen. Nov., Comb. Nov., in the α-Subclass of the Proteobacteria. *Int. J. Syst. Evol. Microbiol. 50*, 1797–1802.
6. Doonan, C. J., Kappler, U., and George, G. N. (2006) Structure of the Active Site of Sulfite Dehydrogenase from *Starkeya Novella*. *Inorg. Chem. 45*, 7488–7492.
7. Kappler, U., and Bailey, S. (2005) Molecular Basis of Intramolecular Electron Transfer in Sulfite-Oxidizing Enzymes is Revealed by High Resolution Structure of a Heterodimeric Complex of the Catalytic Molybdopterin Subunit and a c-Type Cytochrome Subunit. *J. Biol. Chem. 280*, 24999–25007.
8. Kappler, U., and Bailey, S. (2004) Crystallization and Preliminary X-Ray Analysis of Sulfite Dehydrogenase from *Starkeya Novella*. *Acta Crystallogr. D60*, 2070–2072.
9. Hoffmann, C., Ben-Zeev, B., Anikster, Y., Nissenkorn, A., Brand, N., Kuint, J., and Kushnir, T. (2007) Magnetic Resonance Imaging and Magnetic Resonance Spectroscopy in Isolated Sulfite Oxidase Deficiency. *J. Child Neurol. 22*, 1214–1221.
10. Seidahmed, M. Z., Alyamani, E. A., Rashed, M. S., Saadallah, A. A., Abdelbasit, O. B., Shaheed, M. M., Rasheed, A., Hamid, F. A., and Sabry, M. A. (2005) Total Truncation of the molybdopterin/dimerization Domains of SUOX Protein in an Arab Family with Isolated Sulfite Oxidase Deficiency. *Am. J. Med. Genet. A 136*, 205–209.
11. Chiarani, F., Bavaresco, C. S., Dutra-Filho, C. S., Netto, C. A., and Wyse, A. T. (2008) Sulfite Increases Lipoperoxidation and Decreases the Activity of Catalase in Brain of Rats. *Metab. Brain Dis. 23*, 123–132.
12. Zhang, X., Vincent, A. S., Halliwell, B., and Wong, K. P. (2004) A Mechanism of Sulfite Neurotoxicity: Direct Inhibition of Glutamate Dehydrogenase. *J. Biol. Chem. 279*, 43035–43045.
13. Kelly, A., and Stanley, C. A. (2001) Disorders of Glutamate Metabolism. *Mental Retardation and Developmental Disability Research Review 7*, 287–295.
14. Topcu, M., Coskun, T., Haliloglu, G., and Saatci, I. (2001) Molybdenum Cofactor Deficiency: Report of Three Cases Presenting as Hypoxic-Ischemic Encephalopathy. *J. Child Neurol. 16*, 264–270.
15. Karakas, E., Wilson, H. L., Graf, T. N., Xiang, S., Jaramillo-Busquets, S., Rajagopalan, K. V., and Kisker, C. (2005) Structural Insights into Sulfite Oxidase Deficiency. *J. Biol. Chem. 280*, 33506–33515.
16. Kisker, C., Schindelin, H., Pacheco, A., Wehbi, W. A., Garrett, R. M., Rajagopalan, K. V., Enemark, J. H., and Rees, D. C. (1997) Molecular Basis of Sulfite Oxidase Deficiency from the Structure of Sulfite Oxidase. *Cell 91*, 973–983.
17. Feng, C., Kedia, R. V., Hazzard, J. T., Hurley, J. K., Tollin, G., and Enemark, J. H. (2002) Effect of Solution Viscosity on Intramolecular Electron Transfer in Sulfite Oxidase. *Biochemistry 41*, 5816–5821.
18. Feng, C., Kappler, U., Tollin, G., and Enemark, J. H. (2003) Intramolecular Electron Transfer in a Bacterial Sulfite Dehydrogenase. *J. Am. Chem. Soc. 125*, 14696–14697.
19. Feng, C., Tollin, G., and Enemark, J. H. (2007) Sulfite Oxidizing Enzymes. *Biochim. Biophys. Acta 1774*, 527–539.

20. Page, C. C., Moser, C. C., Chen, X., and Dutton, P. L. (1999) Natural Engineering Principles of Electron Tunnelling in Biological Oxidation-Reduction. *Nature 402*, 47–52.
21. Gray, H. B., and Winkler, J. R. (2003) Electron Tunneling through Proteins. *Q. Rev. Biophys. 36*, 341–372.
22. Feng, C., Wilson, H. L., Hurley, J. K., Hazzard, J. T., Tollin, G., Rajagopalan, K. V., and Enemark, J. H. (2003) Essential Role of Conserved Arginine 160 in Intramolecular Electron Transfer in Human Sulfite Oxidase. *Biochemistry 42*, 12235–12242.
23. Pacheco, A., Hazzard, J. T., Tollin, G., and Enemark, J. H. (1999) The pH Dependence of Intramolecular Electron Transfer Rates in Sulfite Oxidase at High and Low Anion Concentrations. *J. Biol. Inorg. Chem. 4*, 390–401.
24. Sullivan, E. P., Jr., Hazzard, J. T., Tollin, G., and Enemark, J. H. (1993) Electron Transfer in Sulfite Oxidase: Effects of pH and Anions on Transient Kinetics. *Biochemistry 32*, 12465–12470.
25. Sullivan, E. P., Jr., Hazzard, J. T., Tollin, G., and Enemark, J. H. (1992) Inhibition of Intramolecular Electron Transfer in Sulfite Oxidase by Anion Binding. *J. Am. Chem. Soc. 114*, 9662–9663.
26. Bailey, S., Rapson, T., Johnson-Winters, K., Enemark, J. H., and Kappler, U. (2009) Molecular Basis for Enzymatic Sulfite Oxidation: How Three Conserved Active Site Residues Shape Enzyme Activity. *J. Biol. Chem. 284*, 2053–2063.
27. Kappler, U., Bailey, S., Feng, C., Honeychurch, M. J., Hanson, G. R., Bernhardt, P. V., Tollin, G., and Enemark, J. H. (2006) Kinetic and Structural Evidence for the Importance of Tyr236 for the Integrity of the Mo Active Site in a Bacterial Sulfite Dehydrogenase. *Biochemistry 45*, 9696–9705.
28. Kappler, U., and McEwan, A. G. (2002) A System for the Heterologous Expression of Complex Redox Proteins in *Rhodobacter capsulatus*: Characterisation of Recombinant Sulphite: Cytochrome c Oxidoreductase from *Starkeya novella*. *FEBS Lett. 529*, 208–214.
29. Kappler, U., Aguey-Zinsou, K. F., Hanson, G. R., Bernhardt, P. V., and McEwan, A. G. (2004) Cytochrome c551 from *Starkeya Novella*: Characterization, Spectroscopic Properties, and Phylogeny of a Diheme Protein of the SoxAX Family. *J. Biol. Chem. 279*, 6252–6260.
30. Lin, J., Balabin, I. A., and Beratan, D. N. (2005) The Nature of Aqueous Tunneling Pathways between Electron-Transfer Proteins. *Science 310*, 1311–1313.
31. Aguey-Zinsou, K., Bernhardt, P. V., Kappler, U., and McEwan, A. G. (2003) Direct Electrochemistry of a Bacterial Sulfite Dehydrogenase. *J. Am. Chem. Soc. 125*, 530–535.
32. Armstrong, F. (2002) Insights from Protein Film Voltammetry into Mechanisms of Complex Biological Electron-Transfer Reactions. *J. Chem. Soc., Dalton Trans.,* 661.
33. Elliott, S. J., McElhaney, A. E., Feng, C., Enemark, J. H., and Armstrong, F. A. (2002) A Voltammetric Study of Interdomain Electron Transfer within Sulfite Oxidase. *J. Am. Chem. Soc. 124*, 11612–11613.
34. Hille, R. (1996) The Mononuclear Molybdenum Enzymes. *Chem. Rev. 96*, 2757–2816.
35. Astashkin, A. V., Johnson-Winters, K., Klein, E. L., Feng, C., Wilson, H. L., Rajagopalan, K. V., Raitsimring, A. M., and Enemark, J. H. (2008) Structural Studies of the Molybdenum Center of the Pathogenic R160Q Mutant of Human Sulfite Oxidase by Pulsed EPR Spectroscopy and ^{17}O and ^{33}S Labeling. *J. Am. Chem. Soc. 130*, 8471–8480.
36. Shih, C., Museth, A. K., Abrahamsson, M., Blanco-Rodriguez, A. M., Di Bilio, A. J., Sudhamsu, J., Crane, B. R., Ronayne, K. L., Towrie, M., Vlcek, A., Jr., Richards, J. H., Winkler, J. R., and Gray, H. B. (2008) Tryptophan-Accelerated Electron Flow through Proteins. *Science 320*, 1760–1762.
37. Nishioka, H., Kimura, A., Yamato, T., Kawatsu, T., and Kakitani, T. (2005) Interference, Fluctuation, and Alternation of Electron Tunneling in Protein Media. 2. Non-Condon Theory for the Energy Gap Dependence of Electron Transfer Rate. *J. Phys. Chem. B 109*, 15621–15635.
38. Nishioka, H., Kimura, A., Yamato, T., Kawatsu, T., and Kakitani, T. (2005) Interference, Fluctuation, and Alternation of Electron Tunneling in Protein Media. 1. Two Tunneling Routes in Photosynthetic Reaction Center Alternate due to Thermal Fluctuation of Protein Conformation. *J. Phys. Chem. B 109*, 1978–1987.
39. Nishioka, H., and Kakitani, T. (2008) Average Electron Tunneling Route of the Electron Transfer in Protein Media. *J. Phys. Chem. B 112*, 9948–9958.
40. Balabin, I. A., Beratan, D. N., and Skourtis, S. S. (2008) Persistence of Structure Over Fluctuations in Biological Electron-Transfer Reactions. *Phys. Rev. Lett. 101*, 158102.

BI801553Q